

# A computational study of magnesium point defects and diffusion in forsterite

Andrew M. Walker<sup>a,\*</sup> Scott M. Woodley<sup>b,c</sup> Ben Slater<sup>b,c</sup>

Kate Wright<sup>d</sup>

<sup>a</sup>*Department of Earth Sciences, University of Cambridge, Downing Street,  
Cambridge, CB2 3EQ, UK*

<sup>b</sup>*Department of Chemistry, 20 Gordon Street, UCL, London, WC1H 0AJ, UK*

<sup>c</sup>*Materials Simulation Laboratory, University College London, London, UK*

<sup>d</sup>*Nanochemistry Research Institute, Department of Applied Chemistry, Curtin  
University of Technology, P.O. Box U1987, Perth 6845, Western Australia*

---

## Abstract

We have studied the formation and migration of point defects within the magnesium sublattice in forsterite using a combination of empirical and quantum mechanical modelling methodologies. Empirical models based on a parameterised force field coupled to a high throughput grid computing infrastructure allow rapid evaluation of a very large number of possible defect configurations. An embedded cluster approach reveals more accurate estimates of defect energetics for the most important defect configurations. Considering all defects in their minimum energy, equilibrium positions, we find that the lowest energy intrinsic defect is the magnesium Frenkel type, where a magnesium atom moves from the M1 site to form a split interstitial defect. This defect has two four coordinated magnesium atoms located outside opposite triangular faces of an otherwise vacant M1 octahedron. The split inter-

stitial defect is more stable than regular interstitials where magnesium is located in either of the two structurally vacant octahedral sites in the hexagonally close packed oxygen lattice. M1 vacancies are also found to form when iron(II) oxidises to iron(III). The energy of the defects away from the equilibrium positions allows the energy barrier to diffusion to be calculated. We have considered the migration of both magnesium vacancies and interstitials and find that vacancies are more mobile. When the contribution from the formation energy of the defects is included we arrive at activation energies for vacancy diffusion that are in agreement with experiment.

*Key words:* forsterite, olivine, magnesium, defect, diffusion

---

## 1 Introduction

2 Although there is a large body of experimental data pertaining to the diffusion  
3 of cations in olivine, there has been no determination of the detailed atomic  
4 scale mechanism by which cationic defects form and move through the crys-  
5 tal lattice. Because of the prevalence of olivine in many mafic and ultramafic  
6 igneous rocks such basic information is valuable in the extrapolation of labo-  
7 ratory measurements of diffusion for use on a wide variety of geological and  
8 geophysical problems. Examples include Fe-Mg exchange in the olivine-spinel  
9 mineral pair, which provides an estimate of cooling rates of ultramafic igneous  
10 rocks, compositional zoning of olivine crystals growing from a melt, the high  
11 temperature mechanism of electrical conductivity of the upper mantle, as well  
12 as the mantle's viscosity and anelasticity.

---

\* Corresponding author.

*Email address:* amw75@cam.ac.uk (Andrew M. Walker).

13 As a relatively simple ternary oxide, cation diffusion in olivine is also of interest  
14 as a model material for the materials scientist. Chemically it forms a complete  
15 solid solution series with compositions ranging between  $\text{Mg}_2\text{SiO}_4$  (forsterite,  
16  $\text{Fo}_{100}$ ) and  $\text{Fe}_2\text{SiO}_4$  (fayalite,  $\text{Fo}_0$ ). The iron-free end member is particularly  
17 useful in this regard with no significant opportunity for redox chemistry or  
18 exchange between the silicon and magnesium sites. Adding iron provides the  
19 possibility for the kind of non-stoichiometry that has been extensively studied  
20 in binary oxides such as iron and nickel oxide (Dieckmann, 1998) and these  
21 processes have been examined in olivine (Smyth and Stocker, 1975; Stocker  
22 and Smyth, 1977; Nakamura and Schmalzried, 1983; Tsai and Dieckmann,  
23 1997, 2002).

24 The olivine structure can be viewed as a distorted hexagonally close packed  
25 (HCP) array of oxygen ions with half of the octahedral sites and one eighth  
26 of the tetrahedral sites occupied by magnesium or iron ions and silicon atoms,  
27 respectively. The distortion of the HCP lattice gives the olivine structure or-  
28 thorhombic symmetry (space group  $Pbnm$ ) and the unit cell contains four  
29 formula units (Figure 1). There are two symmetry distinct octahedral sites:  
30 M1, on a centre of symmetry, and M2, on the mirror plane; one distinct tetra-  
31 hedral site which lies on the mirror plane and three distinct oxygen sites (O1  
32 and O2 on the mirror plane and O3 in a general position). There are also two  
33 vacant octahedral sites, I1 on an inversion center and I2 on the mirror plane.  
34 Iron and magnesium are generally disordered over the two M sites but at low  
35 temperature there is a kinetically hindered tendency to order with iron pref-  
36 erentially occupying the M2 octahedra. This effect has been studied using *in*  
37 *situ* neutron diffraction and the degree of order can be used as an indicator  
38 for cooling rate (e.g. Redfern et al., 1996; Redfern, 1998). The structure can

39 accommodate a range of other cations. For example, calcium is partitioned  
40 onto the M2 site to form monticellite ( $\text{CaMgSiO}_4$ ) and manganese, cobalt and  
41 nickel olivines can be synthesised. There are also a range of isostructural mate-  
42 rials with technological applications. Examples include the olivine phosphates  
43 such as  $\text{LiFePO}_4$  and  $\text{LiCoPO}_4$  which are part of a family of materials with  
44 potential applications as cathodes in batteries (Chung et al., 2002; Islam et al.,  
45 2005).

46 Because of the technological, geological and basic scientific intreats in diffusion  
47 in olivine there has been a large number of experimental studies that give the  
48 diffusion rate of a number of cations in olivine of various compositions. Exper-  
49 imental data includes a series of studies of silicon diffusion (Béjina and Jaoul,  
50 1996; Béjina et al., 2003; Dohmen et al., 2002; Houlier et al., 1988; Sockel  
51 et al., 1980) and many studies of the diffusion of the M site cations includ-  
52 ing magnesium (Bertran-Alvarez et al., 1993; Chakraborty et al., 1994; Sockel  
53 and Hallwig, 1977; Sockel et al., 1980), iron (Bertran-Alvarez et al., 1993;  
54 Chakraborty, 1997; Jaoul et al., 1995; Nakamura and Schmalzried, 1984) and  
55 cobalt (Morioka, 1980). When considering magnesium diffusion, these exper-  
56 iments can be separated into two types, those that measure tracer diffusion  
57 by diffusing  $^{26}\text{Mg}$  into an olivine sample of normal isotopic composition and  
58 those that measure the interdiffusion of magnesium and another element be-  
59 tween two olivine samples of different chemical compositions. The tracer ex-  
60 periments should yield results close to the true self-diffusivity of magnesium  
61 in olivine (there is only a small relative mass difference between  $^{26}\text{Mg}$  and the  
62 normal  $^{24}\text{Mg}$  isotope) while interdiffusion experiments yield some average of  
63 the diffusivities of the two diffusing elements in olivine with an intermediate  
64 composition (see Chakraborty, 1997, for a quantitative discussion).

65 The most complete set of tracer diffusion experiments is that of Chakraborty  
66 et al. (1994) who performed experiments on synthetic crystals of forsterite  
67 as well as natural samples of San-Carlos olivine ( $\text{Fo}_{\approx 90}$ ) at temperatures be-  
68 tween 1000 and 1300 °C under conditions of controlled oxygen fugacity ( $p\text{O}_2$ ).  
69 They give activation energies for magnesium diffusion along [001] of  $400(\pm 60)$   
70  $\text{kJmol}^{-1}$  in forsterite and  $275(\pm 25)$   $\text{kJmol}^{-1}$  in San Carlos olivine and find  
71 that cation diffusion is slower along [010] and [100]. However, no activation  
72 energies in the slow directions are reported. Magnesium diffusivity in San Car-  
73 los olivine was found to vary with  $p\text{O}_2$ , in fact the diffusivity was found to  
74 be directly proportional to  $p\text{O}_2^{1/6}$ . This result, which is in fair agreement with  
75 previous studies (e.g. Nakamura and Schmalzried, 1984, who found diffusivity  
76 to be proportional to  $p\text{O}_2^{1/5.5}$ ), suggests that the diffusing species is a mag-  
77 nesium vacancy charge balanced by the formation of electron holes or by the  
78 oxidation of iron. However, this does not rule out the possibility of diffusion  
79 of magnesium interstitial ions formed with a charge neutrality condition in-  
80 volving magnesium vacancies and singly charged oxygen vacancies (Stocker  
81 and Smyth, 1977). Intriguingly, in the synthetic olivine, the effect of  $p\text{O}_2$  is  
82 less clear, with different samples giving different results. Two possibilities were  
83 put forward, the first invoking a  $p\text{O}_2$  dependent change in the mechanism, and  
84 the second invoking interstitial Fe(III) ions in the charge neutrality condition.  
85 The effect of pressure on magnesium diffusion was also studied and the activa-  
86 tion volume was found to be small and positive (about  $1 \text{ cm}^3\text{mol}^{-1}$ ), which is  
87 similar to the value derived from interdiffusion experiments (Bertran-Alvarez  
88 et al., 1993; Jaoul et al., 1995).

89 Interdiffusion experiments are undertaken by placing two crystals of differing  
90 composition together and studying the process by which the two samples ap-

91 proach chemical equilibrium. Two relevant studies are those of Jaoul et al.  
92 (1995) and Chakraborty (1997) who studied interdiffusion at 600 – 900 °C  
93 and 980 – 1300 °C, respectively. Jaoul et al. (1995) performed their experi-  
94 ments at pressures between 0.5 and 9 GPa in piston-cylinder and multi-anvil  
95 apparatus. They extrapolated their data to 0 GPa and Fo<sub>100</sub> composition and  
96 extracted an activation energy for cation diffusion of 147±58 kJmol<sup>-1</sup> along  
97 [010]. The experiments at higher temperature (Chakraborty, 1997) yielded an  
98 activation energy for cation diffusion along [001] of 226±18 kJmol<sup>-1</sup> for olivine  
99 of composition Fo<sub>86</sub>.

100 The effect of dissolved water on cation diffusion in olivine has recently also  
101 received attention. Experiments by Wang et al. (2004) and Hier-Majumder  
102 et al. (2005) show that magnesium diffusion is at least an order of magnitude  
103 more rapid in olivine containing hydrogen than anhydrous olivine of the same  
104 composition. However, the activation energy for Fe-Mg interdiffusion between  
105 Fo<sub>90</sub> and Fo<sub>80</sub> along [001] was measured as 220±60 kJmol<sup>-1</sup>, little different  
106 from that measured in anhydrous experiments (see Figure 7 of Hier-Majumder  
107 et al., 2005).

108 Although this large body of experimental data is useful for describing the  
109 diffusion controlled processes mentioned above, it does not by itself allow the  
110 nature of the point defects or the detailed mechanisms by which they move to  
111 be determined. In this regard the inherent resolution of atomic scale computer  
112 modelling is a particularly useful approach which can yield crucial details of  
113 the key processes leading to diffusion. Armed with such an understanding we  
114 will be in a much better position to gauge the degree to which experimental  
115 data can safely be extrapolated.

## 116 2 Methodology

117 We make use of two complementary methodologies to study defects and diffu-  
118 sion on the magnesium sub-lattice of forsterite. First, the formation energies  
119 of isolated point defects are studied utilising the Mott-Littleton method with  
120 a parameterised potential model (Catlow, 1977b; Sanders et al., 1984; Lewis  
121 and Catlow, 1985). These calculations were undertaken employing the GULP  
122 code (Gale, 1997; Gale and Rohl, 2003). Further details of the parameters  
123 and computational method used can be found in our previous publication on  
124 oxygen diffusion in olivine (Walker et al., 2003). These parameters, derived  
125 empirically from experimental data for simple binary oxides (supplemented  
126 by quantum mechanical data for the oxygen – oxygen interactions), have been  
127 successfully used for the modelling of the bulk (e.g. Price et al., 1987; Catlow  
128 and Price, 1990) and defect (e.g. Wright et al., 1994; Jaoul et al., 1995; Rich-  
129 mond and Brodholt, 2000; Walker et al., 2005) properties of forsterite and of a  
130 wide range of other silicates. Selected results are then validated using an em-  
131 bedded cluster method. This second method involves modelling the defective  
132 crystal using a quantum mechanical (QM) description of the electronic struc-  
133 ture of the defect and its immediate surroundings coupled to a parameterised  
134 molecular mechanical (MM) model of the crystal further from the defect.

135 For the embedded cluster (QM/MM) calculations we made use of the GUESS  
136 code (Sushko et al., 2000b,a) following the recipe described in Braithwaite  
137 et al. (2002, 2003), Walker et al. (2006) and Berry et al. (2007). Briefly, the  
138 simulation consists of a small inner QM cluster containing 43 ions when no  
139 defects are present, which is embedded within a MM nanocluster of radius  
140 30 Å. In these calculations the inner QM cluster is described using a either

141 Hartree-Fock, Density Functional, or a hybrid B3LYP Hamiltonian using the  
142 Gaussian98 package (Frisch et al., 1998). The MM nanocluster is modelled  
143 using a potential model fitted to be consistent with the QM charges and all  
144 atoms (QM and MM) within 12 Å of the center of the model are allowed to  
145 relax to an energy minimum.

146 The methodology for studying magnesium diffusion by the vacancy mechanism  
147 was identical to that described for oxygen diffusion (Walker et al., 2003) – we  
148 define possible paths that a magnesium ion could take between adjacent M  
149 sites and perform a series of constrained geometry optimizations with the ion  
150 held fixed on this path (between two magnesium vacancies). These calculations  
151 are then used to determine a starting geometry for a transition state search  
152 algorithm based on the Rational Function Optimization (RFO) procedure  
153 described by Banerjee et al. (1985) and implemented in GULP. (A starting  
154 point close to the transition state is needed in order to avoid the optimizer  
155 locating other, less relevant, transition states.) The energy of the defects away  
156 from their equilibrium positions is evaluated using the Mott-Littleton method  
157 and we break diffusion down into a series of “hops” between adjacent sites.  
158 Each hop is associated with a migration energy barrier. By making a series  
159 of hops, the diffusing ion may cross the unit cell. Under the assumption that  
160 consecutive hops are uncorrelated, the maximum migration energy required to  
161 achieve movement in a particular direction is the activation energy for diffusion  
162 in that direction. In order to go beyond the activation energy and extract  
163 the diffusion coefficient would require dynamical information that could be  
164 obtained from lattice dynamics coupled with Vineyard theory (e.g. Vočadlo  
165 et al., 2006). But for a low symmetry structure such as forsterite, further  
166 kinetic Monte Carlo analysis of the results would be required.



167 Because of the apparent complexity of the potential energy surface discovered  
168 in the search for the geometry of magnesium interstitial defects described  
169 in section 3.2, a different approach was used for interstitial diffusion. The  
170 general approach is similar; the potential energy surface is first mapped to  
171 locate approximate saddle points and then an RFO transition state search  
172 is performed, but the method of locating the approximate saddle point is  
173 different. Rather than predetermining individual steps for diffusion, a large  
174 segment of the potential energy surface corresponding to moving the intersti-  
175 tial magnesium ion and relaxing the rest of the structure was evaluated. This  
176 required 2000 separate Mott-Littleton calculations which were completed in  
177 parallel using emerging grid computing technology. In particular we make use  
178 of the large Condor pool at University College London (Wilson et al., 2004),  
179 which harnesses hundreds of teaching computers to provide a significant high  
180 throughput computing resource. Transition states on this surface are then lo-  
181 cated using an iterative basin filling methodology. The approach, described  
182 in more detail by Woodley and Walker (2007), involves the location of the  
183 global minimum followed by incrementally increasing an excess energy and  
184 determining for the volume a diffusing ion with this energy can sample. When  
185 this accessible volume first includes a neighboring periodic image of the global  
186 minimum, a transition state and energy barrier is located.

## 187 **3 Results**

### 188 *3.1 Magnesium vacancies*

189 Using the Mott-Littleton method, the formation energy (energy associated  
190 with removing a single ion from the lattice to an isolated state) of a vacancy  
191 on the M1 site is calculated as 24.5 eV while the formation energy of an  
192 M2 vacancy is 26.4 eV. This means that essentially all magnesium vacancies  
193 should form on the M1 site and the energy difference is in good agreement  
194 with previous calculations using interatomic potentials and periodic Density  
195 Functional Theory (Brodholt, 1997).

196 The embedded cluster calculations, which are limited to calculations of the  
197 M1 vacancy, are in good agreement with the Mott-Littleton results, with cal-  
198 culated defect energy approximately 0.5 eV lower than the Hartree-Fock (HF)  
199 result. This agreement is hardly surprising given that magnesium is an ionic  
200 species in forsterite. Mulliken population analysis of the electron density gives  
201 charges in the region of +2 electronic units, and the parameterised potential  
202 is a good description of a formally charged, spherical closed shell ion.

203 The embedded cluster calculations show few basis set truncation effects (Ta-  
204 ble 1); explicit relaxation with a 6-31+G\* or 6-311+G\* basis set (Foresman  
205 and Frisch, 1996, give an outline of the meaning of these codes) alters the  
206 calculated energy by less than 0.1 eV. Calculations using the HF approxima-  
207 tion give the lowest defect energy while DFT with the PW91 functional gives  
208 the largest defect energy (almost 1 eV higher in energy than the HF result)  
209 suggesting that correlation effects tend to increase the binding of Mg to the

210 forsterite lattice. As expected, the B3LYP hybrid functional yields intermedi-  
211 ate energies.

### 212 3.2 Interstitial defects

213 In practical terms, while vacancies are created by simply removing the relevant  
214 ion from the simulation cell more effort is required to establish the structure of  
215 interstitials. In the case of interstitial magnesium, location of energy minima  
216 was far from straightforward. Initial calculations with interstitial magnesium  
217 ions in either of the two vacant octahedral sites resulted in very large ionic  
218 displacements on relaxation and final defect energies that were very sensitive  
219 to the initial geometry. This is an indication of a failure of the geometry op-  
220 timisation procedure, probably due to a starting configuration away from an  
221 energy minimum on a complex energy hypersurface. In order to locate the  
222 minimum energy configuration for a magnesium interstitial, a large number  
223 of starting geometries were created by placing interstitial magnesium ions on  
224 a regular 0.5 Å grid across the symmetry irreducible portion of the unit cell  
225 and performing an optimisation of all atomic coordinates (including the lo-  
226 cation of the interstitial) using the UCL Condor pool. Following removal of  
227 unphysical structures, where the Coulombic attraction between oxygen ions  
228 and magnesium ions had overcome the short range repulsion leading to very  
229 large negative energies, the lowest energy structures were examined. The low  
230 energy configurations were all split interstitials, where the interstitial ion and  
231 a displaced lattice magnesium ion were located close to opposite faces of an  
232 M1 or M2 octahedron. Embedded cluster calculations show that the split  
233 interstitial is substantially more stable (4.4 eV lower in energy) than an oc-

234 tetrahedrally co-ordinated magnesium interstitial on the I1 site. The reason for  
235 the preference for tetrahedrally co-ordinated magnesium split interstitial de-  
236 fects over octahedrally coordinated interstitial defects on the I1 or I2 site is  
237 not immediately obvious on structural grounds. However, at least part of the  
238 destabilization of octahedral interstitials is due to electrostatic interactions  
239 between the interstitial and the rest of the crystal, which is best described  
240 by the electrostatic potential on the site. We find that this is positive which  
241 explains the low stability of a positively charged magnesium ion on the site  
242 and accounts for the stability of negatively charged, octahedrally coordinated  
243 oxygen interstitials (Walker et al., 2003).

244 The lowest energy site was chosen for further investigation and Mott-Littleton  
245 and embedded cluster calculations were set up with the structure (with two  
246 interstitial ions and a vacancy) as input. The Mott-Littleton approach gave  
247 a formation energy of -17.75 eV and the embedded cluster calculations give  
248 similar values, reported in Table 2. Details of the structure derived from the  
249 embedded cluster calculation is shown in Figure 2. The two magnesium ions  
250 form a split interstitial across the M1 site orientated in the [010] direction  
251 with each magnesium ion in distorted tetrahedral co-ordination, in agreement  
252 with the structure from the Mott-Littleton calculations. The Mg – O bond  
253 distances are similar to those found in crystals with structural magnesium  
254 tetrahedrally co-ordinated by oxygen. For example in a recently synthesised  
255 bismuth magnesium vanadate (Uma and Sleight, 2002) tetrahedral Mg – O  
256 bonds are  $\sim 1.95$  Å long, and in the tetragonal  $\text{Mg}_2\text{TiO}_4$  spinel bond lengths  
257 are 1.995 and 1.981 Å (Millard et al., 1995). In the split interstitial defect the  
258 bonds are 1.89, 2.02, 1.96 and 1.86 Å long for the Mg – O3a, Mg – O1, Mg –  
259 O3b and Mg – O2 bonds, respectively.

260 The energies of the magnesium split interstitial defect calculated using the  
261 QM/MM method and shown in Table 2 are in excellent agreement with the  
262 Mott-Littleton methodology. The HF approximation predicts defect energies  
263 almost 1 eV higher than DFT, while B3LYP and DFT agree to within better  
264 than 0.05%. The Mott-Littleton results fall between those of HF and DFT.  
265 Convergence with basis set size is not as good as in the case of the magnesium  
266 vacancy (perhaps due to the partial occupation of d-orbitals not represented  
267 in the smaller basis sets), but in any case the change in energy from the  
268 6-31+G\*//6-31-G to 6-311+G\*//6-311+G\* is only about 0.1 eV.

### 269 3.3 Diffusion

270 In order to study vacancy diffusion we first defined paths between all adjacent  
271 M sites in the olivine structure. Figure 3 shows the five inequivalent routes  
272 between magnesium vacancies that we consider may be involved in magnesium  
273 vacancy diffusion. Hop A is between two M1 sites along [100] through the  
274 vacant octahedral I1 interstitial position while hop B is between two M2 sites  
275 along [100] through the vacant octahedral I2 position. Hop C is between two  
276 M2 positions with displacement mostly within an (001) plane. Hops D and E  
277 are from M1 sites to M2 sites with D mostly within the (100) plane and E  
278 with significant components in all three crystallographic directions. Hops D'  
279 and E' are the reverse hops from M2 sites to M1 sites. Hop F is between two  
280 M1 sites along [001].

281 Migration energies for each of these hops is given in Table 3, in addition the  
282 transition states for interstitial diffusion are also shown. There are several  
283 points to note. First, the large barriers to diffusion through the vacant I1 and

284 I2 octahedra (hops A and B) is somewhat surprising given the expectation  
285 that magnesium “prefers” an octahedral environment, and especially given  
286 that the transition state is found to be in close to the centre of the octahedron.  
287 It seems likely that this is a Coulombic effect that is also responsible for the  
288 lack of stable octahedrally co-ordinated magnesium interstitials (as described  
289 in section 3.2, above). Vacancy diffusion along [001] is predicted to be via  
290 hop F with the low activation energy of 0.72 eV and diffusion along [100] and  
291 [010] is predicted to be via hops D and C with a extrinsic activation energy  
292 controlled by hop D with a value of 1.98 eV. This is a lower barrier then that  
293 found for interstitial diffusion. Therefore interstitial diffusion is not favoured  
294 over vacancy diffusion in any direction. The energy barrier for hop F has  
295 also been calculated by B ejina et al. (2008) using periodic density functional  
296 theory. These calculations give an upper bound on the barrier height of 0.84  
297 eV, showing that at least this energy barrier is well modeled by the force field  
298 model.

## 299 4 Discussion

300 The defect formation energies presented in the preceding sections represent  
301 the internal energy contribution needed to remove an ion from the lattice to  
302 the gas phase, and to bring an ion from the gas phase, to form vacancies or  
303 interstitials, respectively. Thus this energy does not represent any real process.  
304 However, before considering more realistic defect reactions, we first address the  
305 accuracy of the calculations. As far as we are aware, there is no experimental  
306 data that directly constrains defect thermodynamics although some studies  
307 give important insights. Instead of considering agreement with experiment,

308 the consistency of the present results with previous computational studies will  
309 be considered. Results from the potential model presented in Table 4 (which  
310 includes a summary of the results of this paper) are in excellent agreement with  
311 previous work using the same potential model, this includes work that utilised  
312 the super-cell approach (Richmond and Brodholt, 2000) as well as the Mott-  
313 Littleton method used here (Wright and Catlow, 1994; Jaoul et al., 1995). This  
314 is hardly surprising – indeed disagreement would have suggested errors in one  
315 or more of the codes used to perform the calculations. An additional test of  
316 the accuracy of the potentials based defect energetics is by comparison with  
317 the results of electronic structure calculations. In general, as was pointed out  
318 in the results sections, good agreement with such calculations is observed. In  
319 particular the defect formation energies calculated using the embedded cluster  
320 methodology by Braithwaite et al. (2002, 2003), as well as the additional  
321 results presented here, are in general agreement with the calculated atomistic  
322 values. Discrepancies between results obtained using the potential model and  
323 electronic structure methods, and between results from the embedded cluster  
324 method and periodic DFT calculations, have been noted by Braithwaite et al.  
325 (2003) and Brodholt (1997). The largest error is associated with the formation  
326 of a vacancy on the silicon site. The first reason for this error is likely to be that  
327 the potential model is unable to describe the resultant five co-ordinate silicate  
328 species. A second consideration is that the charge on the silicon vacancy is  
329 the largest considered – resulting in the largest correction terms for the long-  
330 range polarization and the largest electronic polarisation, especially of the  
331 oxygen ions. It is possible that the basis set is not sufficient for modelling this  
332 polarisation. Although some of this difference can be attributed to the small  
333 size of the super-cell it is likely that an additional factor is caused by the way  
334 electronic polarisation around the defect is treated in the atomistic and density

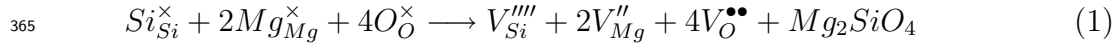
335 functional calculations. In the DFT study it is likely that the polarisation  
336 is under-estimated around the highly charged silicon vacancy because of an  
337 inadequate plane wave basis that was only converged with respect to bulk  
338 olivine (this would destabilise the defect, as it would have a larger effective  
339 charge). On the other hand, the simple shell model used in our potential based  
340 calculations could easily overestimate the polarization of oxygen close to the  
341 defects, which would tend to make the defects too stable.

342 Some additional energies are needed in order to consider the defect reactions,  
343 these include the enthalpy of formation of a number of minerals that will be  
344 the source or sink of the ions from the defect and a number of other standard  
345 energies. These are given in Table 4, with formation energies calculated using  
346 the same interatomic potential model used to calculate the defect structures  
347 and energies.

348 Crystals at thermodynamic equilibrium contain a number of point defects be-  
349 cause the entropy gained in forming the defects outweighs the energetic penalty  
350 of forming the defect. For simple uncharged defects the defect concentration at  
351 a given temperature can be calculated in a straightforward manner. First the  
352 the free energy change in terms of the enthalpy of the formation of the point  
353 defect and the configurational entropy gained as a function of defect concen-  
354 tration is explicitly expressed. Then this expression is differentiated to find  
355 the minimum free energy, giving the equilibrium defect concentration. Such a  
356 procedure is much more complex in multi-component ionic systems because  
357 there are a range of possible defect types. In principle one should minimise  
358 the free energy numerically, taking into account the enthalpic and entropic  
359 contribution from all possible defect species under an imposed condition of  
360 charge neutrality (Ashcroft and Mermin, 1976). The first stage requires the



361 calculation of possible reactions resulting in the formation of intrinsic defects,  
 362 which is undertaken here. Using the results of the Mott-Littleton calculations  
 363 gives the energy of a full Schottky defect where a full formula unit of forsterite  
 364 vacancies is formed and the ions are moved to the surface as:



$$366 \quad E = E(V_{Si}^{''''}) + 2(2V_{Mg1}^{''}) + 4E(V_{O3}^{\bullet\bullet}) + U_{Mg_2SiO_4} = 35.44eV$$

367 or 5.06 eV per defect. This can be compared with a value of 30.25eV given  
 368 by GGA calculated using a super-cell containing 56 atoms (Brodholt, 1997).  
 369 Additional calculations using the same potentials and a fully converged super  
 370 cell gives better agreement with the Mott-Littleton calculations (36.4 eV).  
 371 Decreasing the size of the super cell will tend to reduce this value explaining  
 372 the discrepancy.

373 The second major type of intrinsic defect is the Frenkel defect where a vacancy  
 374 is charge balanced by an interstitial of its own type. In principle, Frenkel  
 375 defects can form on any of the three sublattices. The oxygen Frenkel:



$$377 \quad E = E(O_{I2}^{''}) + E(V_{O3}^{\bullet\bullet}) = 8.43eV$$

378 gives a defect energy of 4.22 eV per defect formed, while the magnesium  
 379 Frenkel:



$$381 \quad E = E(Mg_{I-split}^{\bullet\bullet}) + E(V_{Mg1}^{''}) = 6.73eV$$

382 yields an energy of 3.37 eV per defect, and the silicon Frenkel defect gives:



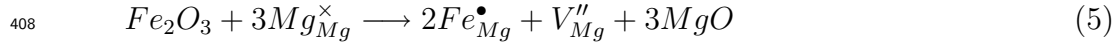
$$384 \quad E = E(Si_I^{\bullet\bullet\bullet\bullet}) + E(V_{Si}^{\prime\prime\prime}) = 24.21eV$$

385 or 12.10 eV per defect. Clearly the Mg Frenkel defect will be the predominant  
386 intrinsic defect, in agreement with the suggestion of Smyth and Stocker (1975),  
387 but this does not rule out the possibility of other intrinsic defects (indeed they  
388 are required to minimise the free energy).

389 The migration energies presented in section 3.3 equate to activation energies  
390 for extrinsic diffusion (in the classical sense), and are within error of the exper-  
391 imental results of Jaoul et al. (1995), after their  $pO_2$  correction. For intrinsic  
392 diffusion (pure  $Mg_2SiO_4$  with thermally created point defects) an appropriate  
393 defect formation energy must be added. Our results suggest that the appro-  
394 priate defect reaction is the magnesium Frenkel defect, and 3.37 eV should  
395 be added to the predicted migration energies to yield the intrinsic activation  
396 energy. This results in activation energies of 5.35 eV ( $513 \text{ kJmol}^{-1}$ ) along [100]  
397 and [010] and 4.09 eV ( $393 \text{ kJmol}^{-1}$ ) along [001], which is within the stated  
398 error of the results of Chakraborty et al. (1994) for higher temperatures where  
399 intrinsic diffusion may be expected. The sense of the anisotropy in activation  
400 energy is also correctly described although no experimental results for the  
401 activation energy along the slow directions have been presented.

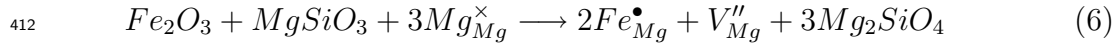
402 For iron bearing olivine Chakraborty et al. (1994) extracted significantly lower  
403 activation energies, presumably because the magnesium vacancies are formed  
404 at lower energetic cost. One way to form magnesium vacancies is to charge  
405 balance their formation with the oxidation of iron, or by the incorporation of

406 ferric iron. Using energies of iron defects calculated by Walker et al. (2003),  
 407 this process can be represented by the reaction:



$$409 \quad E = 2E(Fe_{Mg}^{\bullet}) + E(V_{Mg}'') + 3U(MgO) - U(Fe_2O_3) = 4.47eV$$

410 In the mantle, it would be more realistic for excess MgO to react with pyroxene  
 411 to form olivine:



$$413 \quad E = 2E(Fe_{Mg}^{\bullet}) + E(V_{Mg}'') + 3U(Mg_2SiO_4) - U(Fe_2O_3) - 3U(MgSiO_3) = 3.81eV$$

414 Adding one third of these energies (1.49 or 1.27 eV) to the [001] migration  
 415 energy yields a predicted activation energy of 2.21 or 1.99 eV (213 or 192  
 416  $\text{kJmol}^{-1}$ ), respectively. This is a little lower than the  $275 \pm 25 \text{ kJmol}^{-1}$  mea-  
 417 sured by Chakraborty et al. (1994), but within error of  $226 \pm 18 \text{ kJmol}^{-1}$  mea-  
 418 sured by Chakraborty (1997) for a more iron rich composition.

## 419 5 Conclusions

420 The calculations reported here point to a number of interesting results. First,  
 421 in pure forsterite the majority intrinsic defect species is predicted to be the  
 422 magnesium Frenkel defect. This does not rule out the possibility of defects on  
 423 the silicon or oxygen lattices – indeed these are required at equilibrium – but  
 424 does indicate that electrical conductivity, for example, may be controlled by  
 425 these defects. There has been at least one theoretical study of the intrinsic  
 426 conductivity of forsterite (Morin et al., 1977, 1979), this analysed the likely

427 introduction of bands in the band gap in forsterite on the basis of a comparison  
428 with MgO and quartz. The conclusion was that intrinsic conductivity can be  
429 explained by postulated magnesium interstitials on the unoccupied octahedral  
430 site. The results given above suggest that such defects do not exist and instead  
431 the split interstitial defect should predominate; the need for a re-evaluation  
432 of intrinsic conductivity data is therefore suggested. In any case, electrical  
433 conductivity of olivine under mantle conditions is likely to be controlled by  
434 hydrogen diffusion, which is one reason for the major interest in hydrogen  
435 speciation in upper mantle rocks. In addition to the energies of defects in  
436 forsterite, the defect states in the surrounding minerals should be considered  
437 along with the temperature and pressure. Such an analysis is beyond the scope  
438 of the current work, but the importance of the oxidation and reduction of iron  
439 in the lattice is established.

440 A further interesting observation is that oxygen ions are able to form intersti-  
441 tial defects in the vacant octahedral sites in the olivine structure but, perhaps  
442 surprisingly, magnesium ions are unstable in this environment. The reason  
443 for this seems to be at least partially due to the electrostatic interactions be-  
444 tween the defect and the rest of the crystal, best described by the electrostatic  
445 potential on the site. This is positive, so negatively charged oxygen ions are  
446 stabilised by the electrostatic potential while positively charged magnesium  
447 ions on the site are penalised.

448 The results for magnesium diffusion are in agreement with previous compu-  
449 tational studies Jaoul et al. (1995) and agree to a remarkable degree with the  
450 experimental data. The data of Jaoul et al. (1995) and Chakraborty et al.  
451 (1994) for magnesium diffusion in San Carlos olivine can be interpreted as  
452 the diffusion of magnesium vacancies charge balanced by iron(III) (with the

453 iron oxidation either corrected to extract “true” extrinsic activation energies  
454 or included in the calculation of the activation energy). The higher activation  
455 energy measured by Chakraborty et al. (1994) in synthetic forsterite seems  
456 to indicate that true intrinsic diffusion, with magnesium Frenkel defects pro-  
457 viding the source of vacancies, was measured in that case. The diffusion of  
458 magnesium interstitials is not favoured over vacancy diffusion, a conclusion  
459 reinforced by the many measurements of positive  $pO_2$  dependence of magne-  
460 sium diffusion in olivine.

## 461 **6 Acknowledgments**

462 A.M.W. acknowledges the receipt of a studentship from the Engineering and  
463 Physical Sciences Research Council and K.W. thanks the Royal Society for a  
464 University Research Fellowship.

## 465 **References**

- 466 Ashcroft, N. W., Mermin, N. D., 1976. Solid State Physics. Saunders College,  
467 Orlando.
- 468 Banerjee, A., Adams, N., Simons, J., Shepard, R., 1985. Search for stationary  
469 points on surfaces. *Journal of Physical Chemistry* 89 (1), 52 – 57.
- 470 Béjina, F., Jaoul, O., 1996. Silicon self diffusion in quartz and diopside mea-  
471 sured by nuclear micro-analysis methods. *Physics of the Earth and Plane-  
472 tary Interiors* 97, 145 – 162.
- 473 Béjina, F., Jaoul, O., Liebermann, R. C., 2003. Diffusion in minerals at high  
474 pressure: a review. *Physics of the Earth and Planetary Interiors* 139, 3 – 20.

475 B ejina, F., Blanchard, M., Wright, K., Price, G. D., 2008. A computer simu-  
476 lation study of the effect of pressure on Mg diffusion in forsterite. *Physics*  
477 *of the Earth and Planetary Interiors*, this issue.

478 Berry, A. J., Walker, A. M., Hermann, J., O'Neill, H. S., Foran, G. J., Gale,  
479 J. D., 2007. Titanium substitution mechanisms in forsterite. *Chemical Ge-*  
480 *ology* 242, 176 – 186.

481 Bertran-Alvarez, Y., Jaoul, O., Liebermann, R. C., 1993. Fe-Mg interdiffusion  
482 in single crystal olivine at very high pressure and controlled oxygen fugacity:  
483 technological advances and initial data at 7 GPa. *Physics of the Earth and*  
484 *Planetary Interiors* 70, 102 – 118.

485 Braithwaite, J. S., Sushko, P. V., Wright, K., Catlow, C. R. A., 2002. Hydrogen  
486 defects in forsterite: A test case for the embedded cluster method. *Journal*  
487 *of Chemical Physics* 116 (6), 2628–2635.

488 Braithwaite, J. S., Wright, K., Catlow, C. R. A., 2003. A theoretical study of  
489 the energetics and IR frequencies of hydroxyl defects in forsterite. *Journal*  
490 *of Geophysical Research Solid Earth* 108 (B6), 2284, article number 2284.

491 Brodholt, J. P., 1997. Ab initio calculations on point defects in forsterite  
492 ( $\text{Mg}_2\text{SiO}_4$ ) and implications for diffusion and creep. *American Mineralogist*  
493 82, 1049 – 1053.

494 Catlow, C. R. A., 1977b. Point defect and electronic properties of uranium  
495 dioxide. *Proceedings of the Royal Society of London A.* 353, 533 – 561.

496 Catlow, C. R. A., Price, G. D., 1990. Computer modelling of solid-state inor-  
497 ganic materials. *Nature* 347, 243–247.

498 Chakraborty, S., 1997. Rates and mechanisms of Fe-Mg interdiffusion in  
499 olivine at 980°C - 1300°C. *Journal of Geophysical Research* 102 (B6), 12317–  
500 12331.

501 Chakraborty, S., Farver, J. R., Yund, R. A., Rubie, D. C., 1994. Mg tracer

502 diffusion in synthetic forsterite and San Carlos olivine as a function of P, T  
503 and  $fO_2$ . *Physics and Chemistry of Minerals* 21, 489 – 500.

504 Chung, S. Y., Bloking, J. T., Chiang, Y. M., 2002. Electronically conductive  
505 phospho-olivines as lithium storage electrodes. *Nature Materials* 1 (2), 123–  
506 128.

507 Dieckmann, R., 1998. Point defects and transport in non-stoichiometric oxides:  
508 solved and unsolved problems. *Journal of Physics and Chemistry of Solids*  
509 59 (4), 507–525.

510 Dohmen, R., Chakraborty, S., Becker, H.-W., 2002. Si and O diffusion in  
511 olivine and implications for characterizing plastic flow in the mantle. *Geo-*  
512 *physical Research Letters* 29 (21), 2030.

513 Foresman and Frisch (1996) *Exploring Chemistry with Electronic Structure*  
514 *Methods*. 302 pp. Gaussian Inc. Pittsburgh.

515 Frisch, M. J., Trucks, G. W., Schlegel, H. B., Scuseria, G. E., Robb, M. A.,  
516 Cheeseman, J. R., Zakrzewski, V. G., J. A. Montgomery, J., Stratmann,  
517 R. E., Burant, J. C., Dapprich, S., Millam, J. M., Daniels, A. D., Kudin,  
518 K. N., Strain, M. C., Farkas, O., Tomasi, J., Barone, V., Cossi, M., Cammi,  
519 R., Mennucci, B., Pomelli, C., Adamo, C., Clifford, S., Ochterski, J., Peters-  
520 son, G. A., Ayala, P. Y., Cui, Q., Morokuma, K., Malick, D. K., Rabuck,  
521 A. D., Raghavachari, K., Foresman, J. B., Cioslowski, J., Ortiz, J. V.,  
522 Baboul, A. G., Stefanov, B. B., Liu, G., Liashenko, A., Piskorz, P., Ko-  
523 maromi, I., Gomperts, R., Martin, R. L., Fox, D. J., Keith, T., Al-Laham,  
524 M. A., Peng, C. Y., Nanayakkara, A., Gonzalez, C., Challacombe, M., Gill,  
525 P. M. W., Johnson, B. G., Chen, W., Wong, M. W., Andres, J. L., Head-  
526 Gordon, M., Replogle, E. S., Pople, J. A., 1998. *Gaussian 98* (revision a.7).

527 Gale, J. D., 1997. GULP: A computer program for the symmetry-adapted  
528 simulation of solids. *Journal of the Chemical Society, Faraday Transactions*

529 93 (4), 629 – 637.

530 Gale, J. D., Rohl, A. L., 2003. The general utility lattice program (GULP).  
531 Molecular Simulation 29 (5), 291 – 341.

532 Hier-Majumder, S., Anderson, I. M., Kohlstedt, D. L., 2005. Influence of pro-  
533 tons on Fe-Mg interdiffusion in olivine. Journal of Geophysical Research  
534 110, B02202.

535 Houlier, B., Jaoul, O., Abel, F., Liebermann, R. C., 1988. Oxygen and silicon  
536 self-diffusion in natural olivine. Physics of the Earth and Planetary Interiors  
537 50, 240 – 250.

538 Islam, M. S., Driscoll, D. J., Fisher, C. A. J., Slater, P. R., 2005. Atomic-  
539 scale investigation of defects, dopants and lithium transport in the LiFePO<sub>4</sub>  
540 olivine-type battery material. Chemistry of Materials 17, 5085 – 5092.

541 Jaoul, O., Bertran-Alvarez, Y., Liebermann, R. C., Price, G. D., 1995. Fe-Mg  
542 interdiffusion in olivine up to 9 GPa at T = 600-900°C; experimental data  
543 and comparison with defect calculations. Physics of the Earth and Planetary  
544 Interiors 89, 199 – 218.

545 Lewis, G. V., Catlow, C. R. A., 1985. Potential models for ionic oxides. Journal  
546 of Physics C: Solid State Physics 18, 1149 – 1161.

547 Millard, R. L., Peterson, R. C., Hunter, B. K., 1995. Study of the cubic to  
548 tetragonal transition in Mg<sub>2</sub>TiO<sub>4</sub> and Zn<sub>2</sub>TiO<sub>4</sub> spinells by <sup>17</sup>O MAS NMR  
549 and Rietveld refinement of X-ray diffraction data. American Mineralogist  
550 80, 885 – 896.

551 Morin, F. J., Oliver, J. R., Housley, R. M., 1977. Electrical properties of  
552 forsterite, Mg<sub>2</sub>SiO<sub>4</sub>. Physical Review B 16 (10), 4434 – 4445.

553 Morin, F. J., Oliver, J. R., Housley, R. M., 1979. Electrical properties of  
554 forsterite, mg<sub>2</sub>sio<sub>4</sub> II. Physical Review B 19 (6), 2886 – 4445.

555 Morioka, M., 1980. Cation diffusion in olivine - i. cobalt and magnesium.



556 Geochimica et Cosmochimica Acta 44, 759 – 763.

557 Nakamura, A., Schmalzried, H., 1983. On the nonstoichiometry and point  
558 defects of olivine. Physics and Chemistry of Minerals 10 (1), 27 – 37.

559 Nakamura, A., Schmalzried, H., 1984. On the  $\text{Fe}^{2+}$  -  $\text{Mg}^{2+}$  interdiffusion in  
560 olivine (II). Berichte der Bunsen Gesellschaft für Physikalische Chemie 88,  
561 140 – 145.

562 Price, G. D., Parker, S. C., Leslie, M., 1987. The lattice dynamics of forsterite.  
563 Mineralogical Magazine 51, 157 – 170.

564 Redfern, S. A. T., 1998. Time-temperature-dependent M-site ordering in  
565 olivines from high-temperature neutron time-of-flight diffraction. Physica  
566 B 141, 1189–1196.

567 Redfern, S. A. T., Henderson, C. M. B., Wood, B. J., Harrison, R. J., Knight,  
568 S. K., 1996. Determination of olivine cooling rates from metal-cation order-  
569 ing. Nature 381, 407 – 409.

570 Richmond, N. C., Brodholt, J. P., 2000. Incorporation of  $\text{Fe}^{3+}$  into forsterite  
571 and wadsleyite. American Mineralogist 85 (9), 1155–1158.

572 Sanders, M. J., Leslie, M., Catlow, C. R. A., 1984. Interatomic potentials for  
573  $\text{SiO}_2$ . Journal of the Chemical Society, Chemical Communications.

574 Smyth, D. M., Stocker, R. L., 1975. Point defect and non-stoichiometry in  
575 forsterite. Physics of the Earth and Planetary Interiors 10, 183 – 192.

576 Sockel, H. G., Hallwig, D., 1977. Ermittlung kleiner Diffusionskoeffizienten  
577 mittels SIMS in oxydischen Verbindungen. Mikrochimica Acta Suppl. 7, 95–  
578 107.

579 Sockel, H. G., Hallwig, D., Schachtner, R., 1980. Investigations of slow ex-  
580 change processes at metal and oxide surfaces and interfaces using secondary  
581 ion mass spectrometry. Materials science and engineering 42, 59 – 64.

582 Stocker, R. L., Smyth, D. M., 1977. Effect of enstatite activity and oxygen

583 partial pressure on the point-defect chemistry of olivine. *Physics of the*  
584 *Earth and Planetary Interiors* 16, 145–156.

585 Sushko, P. V., Shluger, A. L., Baetzold, R. C., Catlow, C. R. A., 2000a. Em-  
586 bedded cluster calculations of metal complex impurity defects: properties of  
587 the iron cyanide in NaCl. *Journal of Physics: Condensed Matter* 12, 8257 –  
588 8266.

589 Sushko, P. V., Shluger, A. L., Catlow, C. R. A., 2000b. Relative energies of  
590 surface and defect states: ab initio calculations for the MgO (001) surface.  
591 *Surface Science* 450, 153–170.

592 Tsai, T.-L., Dieckmann, R., 1997. Point defects and transport of matter and  
593 charge in olivines,  $(\text{Fe}_x\text{Mg}_{1-x})_2\text{SiO}_4$ . *Materials Science Forum* 239 - 241,  
594 399 – 402.

595 Tsai, T.-L., Dieckmann, R., 2002. Variation of the oxygen content and point  
596 defects in olivines,  $(\text{Fe}_x\text{Mg}_{1-x})_2\text{SiO}_4$ ,  $0.2 \leq x \leq 1.0$ . *Physics and Chemistry*  
597 *of Minerals* 29, 680 – 694.

598 Uma, S., Sleight, A. W., 2002. A new bismuth magnesium vanadate with  
599 reduced vanadium:  $\text{BiMg}_{2.5}\text{V}_{18.5}\text{O}_{38}$ . *Journal of Solid State Chemistry* 164,  
600 138 – 143.

601 Vočadlo, L., Wall, A., Parker, S. C., Price, G. D. 1995. Absolute ionic diffusion  
602 in MgO – computer calculations via lattice dynamics. *Physics of the Earth*  
603 *and Planetary Interiors* 88, 193 – 210.

604 Walker, A. M., 2004. Computational studies of point defects and dislocations  
605 in forsterite ( $\text{Mg}_2\text{SiO}_4$ ) and some implications for the rheology of mantle  
606 olivine. PhD, University of London.

607 Walker, A. M., Demouchy, S., Wright, K., 2006. Computer modelling of the  
608 energies and vibrational properties of hydroxyl groups in  $\alpha$ - and  $\beta$ - $\text{Mg}_2\text{SiO}_4$ .

609 European Journal of Mineralogy 18, 529 – 543.

610 Walker, A. M., Gale, J. D., Slater, B., Wright, K., 2005. Atomic scale mod-  
611 elling of the cores of dislocations in complex materials part 2: applications.  
612 Physical Chemistry Chemical Physics 7.

613 Walker, A. M., Wright, K., Slater, B., 2003. A computational study of oxygen  
614 diffusion in olivine. Physics and Chemistry of Minerals 30 (9), 536 – 545.

615 Wang, Z. Y., Hiraga, T., Kohlstedt, D. L., 2004. Effect of H<sup>+</sup> on Fe-Mg in-  
616 terdiffusion in olivine, (Fe,Mg)<sub>2</sub>SiO<sub>4</sub>. Applied Physics Letters 85 (2), 209 –  
617 211.

618 Wilson, P., Emmerich, W., Brodholt, J., 2004. Leveraging HTC for UK  
619 eScience with very large Condor pools: Demand for transforming untapped  
620 power into results. In: Proceedings of the UK e-Science All Hands Meeting  
621 2004.

622 Woodley, S. M., Walker, A. M., 2007. New software for finding transition states  
623 by probing accessible, or ergodic, regions. Molecular Simulation 33, 1229 –  
624 1231.

625 Wright, K., Catlow, C. R. A., 1994. A computer simulation study of (OH)  
626 defects in olivine. Physics and Chemistry of Minerals 20, 515 –518.

627 Wright, K., Freer, R., Catlow, C. R. A., 1994. The energetics and structure of  
628 the hydrogarnet defect in grossular: a computer simulation study. Physics  
629 and Chemistry of Minerals 20, 500 – 503.

Table 1

Defect energies for Mg1 vacancies in forsterite calculated using the embedded cluster method. The basis set code refers to the basis used for geometry optimisation and final energy calculation respectively (so 6-31+G\*//6-31G means optimisation using the 6-31G basis with final energy calculation using the 6-31+G\* basis). Rapid convergence is observed for each method with basis set size.

Basis set	Defect energy (eV)		
	Hartree-Fock	DFT (PW91)	DFT (B3LYP)
6-31G//6-31G	25.832	27.127	26.875
6-31+G*//6-31G	24.942	25.725	25.564
6-31+G*//6-31+G*	24.979	25.762	25.610
6-311+G*//6-31+G*	25.002	25.780	25.632
6-311+G*//6-311+G*	25.017	25.773	25.625

Table 2

Defect energies for the magnesium split interstitial across the M1 site. The meaning of the basis set symbols are given in the caption to Table 1.

Basis set	Defect energy (eV)		
	Hartree- Fock	DFT (PW91)	DFT (B3LYP)
6-31G//6-31G	-18.029	-18.470	-18.478
6-31+G*//6-31G	-17.366	-17.952	-17.947
6-31+G*//6-31+G*	-17.403	-18.001	-17.993
6-311+G*//6-31+G*	-17.503	-18.045	-18.038
6-311+G*//6-311+G*	-17.508	-18.049	-18.043

Table 3

Migration energies for magnesium vacancy and interstitial diffusion in forsterite.

Hop	Defect energy of initial state (eV)	Defect energy of activated state (eV)	Migration energy (eV)
A	24.48	30.37	5.89
B	26.40	35.50(a)	9.10
C	26.40	27.87(a)	1.47
D	24.48	26.46	1.98
D'	26.40		0.06
E	24.48	30.94(a)	4.54
E'	26.40		6.64
F	24.40	25.12	0.72
Interstitial // [100]	-17.75	-13.86	3.89
Interstitial // [010]	-17.75	-13.86	3.89
Interstitial // [001]	-17.75	-14.62	3.13

(a) These failed to converge in the RFO part of the calculation and so an estimate of the transition state is made from the initial search, where the moving ion is fixed and the rest of the structure relaxed, is used, the true energy of the activated state is not expected to be significantly different from this estimate.

Table 4

Defect energies for a range of possible intrinsic defects in forsterite

Defect <sup>a</sup>	Mott-Littleton method (eV)
$V_{O1}^{\bullet\bullet}$	27.97 <sup>b</sup>
$V_{O2}^{\bullet\bullet}$	25.20
$V_{O3}^{\bullet\bullet}$	24.54
$O''_{I(1)}$	-14.37
$O''_{I(2)}$	-16.11
$V''_{Mg1}$	24.48
$V''_{Mg2}$	26.40
$Mg^{\bullet\bullet}_{I(split)}$	-17.75
$V''''_{Si}$	100.81 <sup>c</sup>
$Si_I^{\bullet\bullet\bullet\bullet}$	-76.60
$Fe^{\bullet}_{M1}$	-22.55 <sup>d</sup>
$Fe^{\bullet}_{M2}$	-23.24
$U(Mg_2SiO_4)$	-212.49
$U(MgSiO_3)$	-171.97
$U(Fe_2O_3)$	-150.37
$U(MgO)$	-41.31

<sup>a</sup> Defects are described using Kröger-Vink defect notation and include vacancies in all three oxygen positions, oxygen interstitial ions occupying both free octahedral sites on both magnesium sites, a split interstitial magnesium defect, a silicon vacancy and a silicon interstitial. Defect energies are quoted with respect to the perfect forsterite lattice and the ion at infinity.

<sup>b</sup> Energies of oxygen defects are from Walker et al. (2003)

<sup>c</sup> Energies of silicon defects are from Walker (2004)

<sup>d</sup> Energies of iron defects are from Walker et al. (2003)

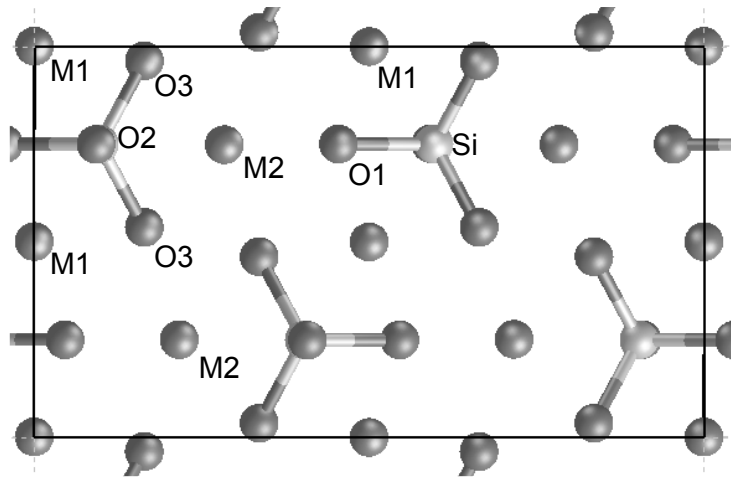


Fig. 1. Unit cell of the olivine structure viewed along [100]. The long visible cell axis is [010] and the shorter one is [001], occupied sites are marked.



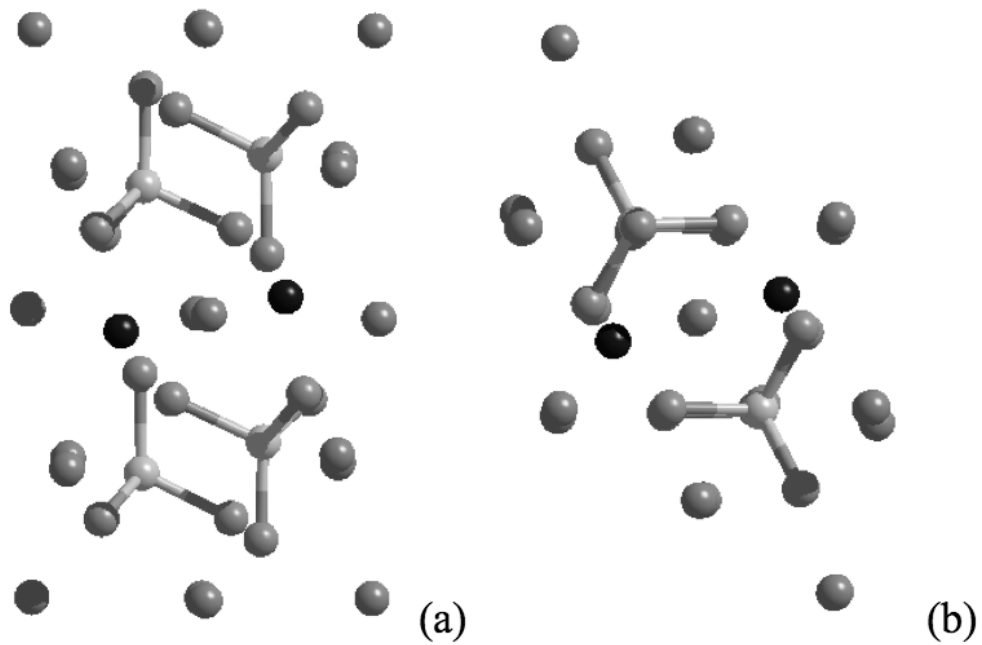


Fig. 2. Structure of magnesium split interstitial defect from embedded cluster calculations. (a) Looking along  $[010]$  with  $[100]$  oriented up the page. (b) Looking along  $[100]$  with  $[001]$  oriented up the page. The two tetrahedral magnesium ions are shown in black, otherwise magnesium ions isolated spheres, silicon and oxygen ions form  $\text{SiO}_4$  tetrahedra.

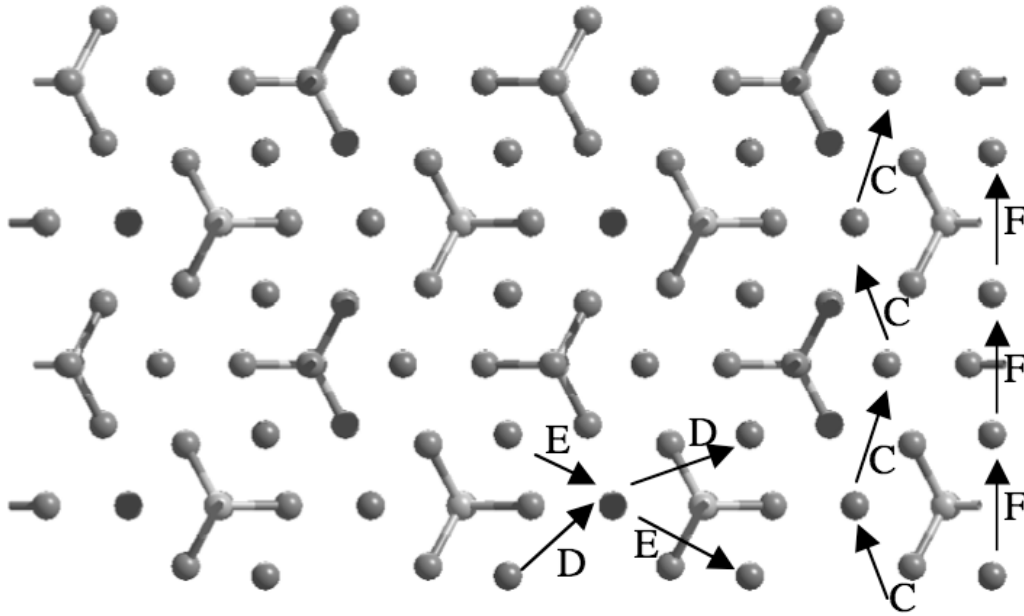


Fig. 3. Magnesium diffusion by the vacancy mechanism (see text for details) projected onto the (100) plane. Hops A and B are not shown as they are perpendicular to the plane.